Published in final edited form as:
*Adv Drug Deliv Rev*. 2010 March 8; 62(3): 329–338. doi:10.1016/j.addr.2009.11.005.

# Modified natural nanoparticles as contrast agents for medical imaging

**David P. Cormode**[1], **Peter A. Jarzyna**[1], **Willem J. M. Mulder**[1], and **Zahi A. Fayad**[1,*]

[1] Translational and Molecular Imaging Institute, Mount Sinai School of Medicine, One Gustave L. Levy Place, Box 1234, New York, NY 10029

## Abstract

The development of novel and effective contrast agents is one of the drivers of the ongoing improvement in medical imaging. Many of the new agents reported are nanoparticle-based. There are a variety of natural nanoparticles known, e.g. lipoproteins, viruses or ferritin. Natural nanoparticles have advantages as delivery platforms such as biodegradability. In addition, our understanding of natural nanoparticles is quite advanced, allowing their adaptation as contrast agents. They can be labeled with small molecules or ions such as $Gd^{3+}$ to act as contrast agents for magnetic resonance imaging, $^{18}F$ to act as positron emission tomography contrast agents or fluorophores to act as contrast agents for fluorescence techniques. Additionally, inorganic nanoparticles such as iron oxide, gold nanoparticles or quantum dots can be incorporated to add further contrast functionality. Furthermore, these natural nanoparticle contrast agents can be rerouted from their natural targets via the attachment of targeting molecules. In this review, we discuss the various modified natural nanoparticles that have been exploited as contrast agents.

### Keywords

Nanoparticles; contrast agents; medical imaging; lipoproteins; viruses; MRI

## 1 Introduction

Medical imaging has undergone tremendous improvements over the last 35 years, with the introduction of techniques such as magnetic resonance imaging (MRI) [1], computed tomography (CT) [2] and other developments that allow non-invasive and accurate diagnoses. Asides from anatomical information, data on a wide variety of processes can be derived from medical imaging, such as diffusion [3], inflammation [4] and angiogenesis [5,6]. Contrast agents are prerequisite in some imaging techniques, facilitate the acquisition of new data and novel or improved contrast agents are an important research topic. Nanoparticles that incorporate contrast-generating materials are an especially strong focus of recent contrast agent research [7–12]. Nanoparticles offer several attractions as contrast agents, including improved contrast, carrying high payloads, long circulation times and the ease of including multiple properties [13].

*Corresponding author: Tel: 212-241-6858, Fax: 240-368-8096, Zahi.Fayad@mssm.edu.

Paramagnetic or superparamagnetic materials induce MRI contrast, so MR-active nanoparticles are normally labeled with gadolinium ions ($Gd^{3+}$) [14] or contain iron oxide cores [15]. Nuclear-based imaging techniques such as positron-emission tomography require radioactive elements in their contrast agents. Quantum dots have excellent properties for fluorescence based imaging techniques [16] and are widely used in pre-clinical research. CT relies on the attenuation of x-rays and therefore nanoparticulate contrast agents for this imaging technique have been based on heavy elements such as gold [17,18], bismuth [19] or iodine [20,21]. Many synthetic nanoparticles that contain these contrast generating materials have now been reported, such as micelles, liposomes, microemulsions, iron oxides, gold nanoparticles, silica, or carbon nanotubes [10,22–26]. Great efforts have been devoted to developing coatings for these synthetic nanoparticles that are biocompatible, yield long-circulation times, low levels of opsonization and have low toxicities, for medical imaging but for other applications as well. The substances used for this purpose include polymers such as polyethylene glycol [27], phospholipids [28] and dextran [29].

Although much of the research in nanotechnology has focused on man-made materials, Nature created a variety of nanoparticles over the eons, such as lipoproteins, viruses and ferritin. These nanoparticles play important roles in the physiology of many organisms and in disease processes such as atherosclerosis and infections. While investigating the interactions of natural nanoparticles in biology, knowledge of their structure and function has been built up. As a result, various researchers have come to the realization that these natural nanoparticles can be harnessed as delivery vehicles for contrast generating materials, as an alternative to synthetic nanoparticle systems. The advantages of natural nanoparticles include precisely defined dimensions, possible evasion of the immune system, biocompatibility and biodegradability. In comparison, artificial nanoparticles may be swiftly opsonized and cleared by the immune system, contain toxic materials or be non-biodegradable. Asides from acting as effective contrast agents, labeled natural nanoparticles can be used to produce greater knowledge of their properties by imaging their distribution *in vivo.* As we will explain in this review, methods for including contrast generating materials in natural nanoparticles for the majority of medical imaging techniques have been developed.

For this review we define a natural nanoparticle as an assembly of molecules and atoms that has at least one dimension in the 1–100 nm size range. Therefore we exclude macromolecules such as human serum albumin or biological species on the micron-scale such as cells, both of which can be labeled with contrast generating materials [30,31]. The main categories of natural nanoparticles we will discuss are lipoproteins, viruses and ferritin, whose composition and the contrast agents that have been based on them will be described.

## 2 Lipoproteins

Lipoproteins are divided into five categories: high density lipoproteins (HDL), low density lipoproteins (LDL), intermediate density lipoprotein (IDL), very low density lipoproteins (VLDL) and chylomicrons. The ‘density’ nomenclature derives from the density gradient centrifugation procedure originally used to separate these nanoparticles [32]. In this procedure serum from blood is ultracentrifuged with increasing densities of KBr solution, yielding hundreds of milligrams of each lipoprotein from each liter of plasma. The supply of human plasma available from blood banks is relatively plentiful or plasma can be donated especially for lipoprotein experiments. The lipoproteins share the same basic structure: a hydrophobic core of triglycerides and cholesterol esters that is covered with a phospholipid/cholesterol mixed layer, into which apolipoproteins are embedded (Figure 1A). Apolipoproteins are a class of amphiphatic proteins that are found in lipoproteins [33]. They integrate in the lipoprotein assembly in such a way that hydrophobic regions bind to the hydrophobic tails of the phospholipids and the hydrophobic core, while the other hydrophilic face of the protein is

oriented towards water. Several of them have been isolated and letters and numbers in their nomenclature distinguish them, for example the major protein constituent of HDL is apolipoprotein A-I, abbreviated as apoA-I. The proteins can range quite widely in size with apoA-I consisting of 243 amino acid residues while apoB100, the major protein of LDL, consists of 4536 amino acids. Asides from density and protein content, the lipoproteins also vary in diameter, with HDL the smallest, falling in the 7–13 nm size range, while LDL is in the size range of 22–27 nm, followed by IDL (27–30 nm) and VLDL (35–80 nm). Lipoproteins in a size range of 80–1200 nm are referred to as chylomicrons [34].

The primary function of lipoproteins in the body is transporting cholesterol and other lipids. The apolipoprotein portions of the particles bind to cell membrane proteins to facilitate transfer of lipids [35,36]. Generally speaking, HDL removes lipids such as cholesterol from tissues and transfers it to the liver for redistribution to other tissues or for excretion. The other lipoproteins deliver lipids to tissues. Lipoproteins have additional known functions, for example HDL is known to be anti-inflammatory [37]. HDL and LDL are highly involved in atherosclerosis, the build-up of fatty deposits in the arteries. High LDL levels have been shown to lead to more advanced atherosclerotic lesions in patients, and LDL is thought to deposit in the arteries [38], causing atherosclerosis to develop. Elevated HDL levels lead to lesser lesions and therefore is termed ‘atheroprotective’ [39]. Lowering LDL levels has been effectively achieved through use of a class of drug known as statins [40] while raising HDL levels is a goal of several pharmaceutical companies [41]. As a consequence of the importance of lipoproteins in biology, it is attractive to image their distribution in the body. Furthermore, when modified as contrast agents, it is possible to exploit the natural interactions of the lipoproteins with cell membrane proteins to perform specific imaging. For example, LDL may be used to detect cancer as the LDL receptor is overexpressed in some cancers [42].

Two approaches have been taken to label lipoproteins so they act as contrast agents (Figure 1B). First, contrast generating materials can be included in the coating of the particle. This can be done by attaching contrast generating atoms to the protein constituent of the lipoprotein [43] or by including specially modified amphiphiles in the formulation [44]. Lipoprotein contrast agents containing unstable nuclei (e.g. $^{123}$I for nuclear imaging techniques [43]), chelated paramagnetic ions (i.e. gadolinium for MRI [44]) and fluorophores (for fluorescence imaging techniques [45]) have been synthesized via these routes. Second, contrast generating materials or drugs may be loaded in the hydrophobic core of lipoproteins. Examples of this include nanocrystals replacing the triglyceride and cholesterol ester core of HDL [18] to create nanoparticles that are contrast agents for MRI, CT or optical imaging, as well as the inclusion of paclitaxel in HDL so the particle acts as an anti-cancer therapeutic [46]. Both the approaches of including contrast generating materials in the lipoprotein coating and in the core can be combined to create nanoparticles that yield contrast for multiple imaging modalities [18]. Lipoproteins can be further modified to target receptors that they do not naturally interact with, for example folic acid residues have been appended to the lysine residues of apoB in LDL, making the nanoparticle specific for cells that over-express the folate receptor [47]. Therefore lipoproteins can be modified to 1) generate contrast for a wide variety of imaging techniques and 2) be specific for various cell types or pathologies. Taking all these factors together, it is clear that lipoproteins are well suited for development as contrast agents. In the following sections we will outline the contrast agents that have been reported for the different lipoproteins.

### 2.1 High density lipoprotein

Shaish et al were the first to modify HDL as a contrast agent [48]. In their study HDL was modified with $^{125}$I and injected into atherosclerotic mice. The radiolabeled HDL allowed the investigation of the blood clearance and organ distribution of this lipoprotein. The aortas of

mice injected with this agent were excised and imaged using autoradiography, where it was seen that the agent accumulated mostly in the aorta arch, in areas near the renal arteries and the bifurcation, correlating with regions where atherosclerotic plaque develops most extensively [49].

Subsequently, Frias et al reported HDL modified with gadolinium chelating phospholipids to provide MRI contrast and with a fluorophore labeled phospholipid to enable their visualization with confocal microscopy [44,50]. The synthesis of HDL labeled with these lipids can be achieved through a variety of methods, including the cholate dialysis method, incubation methods and sonication [51]. This gadolinium labeled HDL (Gd-HDL) was injected into atherosclerotic mice and MR imaging pre- and 24 hours post-injection revealed accumulation of the agent in the abdominal aortas of the mice. The accumulation occurred in areas where plaque had developed, as shown by histology and confocal microscopy revealed that the agent had gathered in macrophage cells. Imaging of this cell type in atherosclerosis is attractive, as the level of macrophage cells in plaque has been associated with the probability of plaque rupture and adverse clinical events [52]. Recently an HDL-based nanoparticle was reported where novel gadolinium-chelating lipids were used so that the longitudinal relaxivity (a measure of the MRI contrast produced) was 4 times higher than of the previous version [53].

A synthetic version of this gadolinium-labeled HDL platform was developed by Cormode et al who substituted the apolipoprotein constituent of the nanoparticle with either a 37 or 18 amphiphatic amino acid peptide, both of which mimic the behavior of apoA-I and [54,55]. Fluorescent imaging experiments showed these ‘synthetic’ HDL nanoparticles to be taken up by macrophage cells in a receptor dependant manner, indicating that they could have potential for MR imaging of this cell type. Accordingly, both types of synthetic HDL were applied in atherosclerotic mice and produced an increase in contrast of about 90% in the aorta. The blood half-life and biodistribution of the agents were found to be similar and therefore the synthetic HDL based on each peptide was found to be equally effective for macrophage imaging.

As well as modifying the coating of HDL, the core composition can be altered by the incorporation of contrast-generating materials. Assemblies of labeled phospholipids, hydrophobically coated inorganic nanocrystals and apoA-I formed HDL with contrast generating materials in the core and the coating [18]. The inorganic nanocrystals used in this study were gold, iron oxide and quantum dots, which provide contrast for CT, MRI and fluorescence techniques respectively. The gold core HDL was referred to as Au-HDL, the iron oxide HDL as FeO-HDL and the quantum dot HDL as QD-HDL. By including paramagnetic and/or fluorescent phospholipids in the coating of the particles each was additionally made active for MRI and fluorescence techniques (Figure 2A). Analysis of the size, protein content and macrophage efflux (a bioassay of HDL function, unpublished data), showed that these nanocrystal-core particles were very similar to native HDL. Confocal microscopy, MRI, CT, TEM and fluorescence imaging (Figure 2B) were carried out on macrophage cells incubated with nanocrystal HDL. The cells took up the contrast agents avidly and the multifunctional nature of the particles was established as contrast was provided for each imaging technique. The particles were applied to atherosclerotic mice, for which uptake in the aorta was demonstrated *in vivo* via MRI and *ex vivo* via CT and fluorescence imaging (Figure 2C-F). Confocal microscopy demonstrated the accumulation of nanocrystal-HDL in macrophages.

To improve the targeting of HDL to macrophages, Chen et al reported gadolinium and fluorophore labeled HDL that had a lipopeptide, P2A2, included in the phospholipid coating [56]. The sequence of this peptide was derived from the LDL receptor binding domain of apolipoprotein E and has been shown to promote cellular uptake of lipid based particles [57]. It was theorized that inclusion of the P2A2 lipopeptide would improve the uptake of HDL contrast agents in macrophages. This was shown to be the case *in vitro* via fluorescence

techniques and MRI experiments and *in vivo* by the elevated level of contrast in MR images of the plaques of mice injected with P2A2-Gd-HDL as compared to those of mice injected with Gd-HDL.

### 2.2 Low density lipoprotein

Since the 1980s there have been several reports of LDL labeled with unstable nuclei and applied for nuclear imaging techniques. The unstable nuclei used include $^{123}$I, $^{125}$I, $^{111}$In, $^{19}$F and $^{99m}$Tc [43,48,58–60]. For example, Ginsberg et al labeled LDL with $^{99m}$Tc via reductive coupling of 99m-pertechnetate with LDL isolated from patients [60]. In this study, $^{99m}$Tc-LDL was injected into a normal patient and patients with lipid disorders. The subjects with lipid disorders bore xanthomas, which are bulbous accumulations of lipids in the skin and tendons of such patients. Gamma camera images of the patients at 4 and 24 hours revealed significant uptake of the $^{99m}$Tc-LDL in the xanthomas (Figure 3A), indicating that the LDL was taken up by these pathological tissues.

More recently Zheng et al modified LDL with the DiI fluorophore intercalated in the phospholipid layer and folic acid (FA) attached to lysine residues on apoB, the major apolipoprotein component of LDL [47]. The addition of FA re-routed the LDL from its natural targets as demonstrated by the fluorescence observed in confocal microscopy images of cancer cells that highly express the folate receptor incubated with the modified agent. FA-LDL, labeled with near-infrared dye DiR (Figure 3B) was applied *in vivo* to mice inoculated with two tumors, one on the right flank that over-expressed the folate receptor (KB) and another on the left flank that did not (HT1080) [45]. Fluorescence imaging of these mice resulted in preferential accumulation of the agent in the KB tumor indicating that the folate targeting was successful *in vivo* (Figure 3C).

LDL has been labeled with manganese(II) ions coordinated in a porphyrin molecule [62]. Manganese(II) ions have five unpaired electrons, are hence highly paramagnetic and can act as contrast agents for MRI. This Mn-labeled LDL was incubated with foam cells, a pathogenic cell type in atherosclerosis. These incubations resulted in a reduction of the $T_1$ (an MRI parameter) of these cells to 443 ms from 661 ms when the cells were untreated, which indicates that Mn-LDL could act as a contrast agent for atherosclerosis. There are several reports where LDL has been labeled with gadolinium. In the first of which, 50 gadolinium chelates were integrated into the phospholipid layer of the nanoparticle and MR imaging was performed on mice injected with this contrast agent [63]. Less contrast was observed in the liver of mice genetically engineered to not possess the LDL receptor, as compared to mice that did, indicating that gaolinium modified LDL still binds to this receptor. The same group later reported LDL loaded with gadolinium via a different methodology, leading to as many as 500 gadolinium chelates per particle [61]. These nanoparticles were found to be effective for MR imaging of tumors that highly express the LDL receptor in a mouse model, with a 26% increase in contrast at 24 hours post-injection (Figure 3D). Geninatti Crich et al reported LDL labeled with a fluorophore and a novel gadolinium chelate, Gd-AAZTA, which produces elevated levels of MR contrast [42]. This Gd-AAZTA-LDL was also shown to be effective for MR imaging tumors *in vivo* and areas of high MR contrast in the tumor correlated with areas of high fluorescence as shown by confocal microscopy performed on sections of the tumor. This result confirmed that the MR contrast observed in the tumor was due to accumulation of Gd-AAZTA-LDL.

### 2.3 Very low density lipoprotein and chylomicrons

VLDL has been labeled with $^{123}$I and used to investigate the behavior of this lipoprotein *in vivo* via gamma camera imaging [64]. Chylomicron-type particles have been loaded with iodinated triglyceride molecules to act as a CT contrast agent [65]. These were applied in dogs

for lymph node imaging, in which organ an increase in attenuation as high as 155 Hounsfield units was observed post-injection [66].

## 3 Viruses

There are a wide variety of viruses, but they share the common structure of a shell composed of protein subunits that encloses either DNA or RNA. They range widely in size and shape, with the cowpea chlorotic mottle virus being a 28 nm spheroid (Figure 4A-C) and the tobacco mosaic virus being an 18 by 300 nm rod, as examples [67]. Their natural function is to enter the cells of other organisms, produce copies of themselves, then leave to infect other cells. A well-known example of this is the human immunodeficiency virus or HIV, but there are viruses that target most types of organisms and it is estimated that viruses are the second most prevalent biological entity on the planet [68]. Large quantities of viruses can be synthesized using relatively straightforward methodology. For example, the cowpea mosaic virus (CPMV) can be synthesized using a simple infection procedure that produces effective propagation in the host, a high yield of virus particles (1–2 g per 1 kg of infected leaf material) [69] and purified using a simple method. Synthesis of the virus is initiated by mechanically introducing infectious cDNA clones encoding the viral genome or virus containing solutions (infectious particles in buffer extracts or sap from infected plants) onto cowpea plants. After extraction from the plant leaves, the purification of the virus can be accomplished by sucrose cushion ultracentrifugation [70]. A good yield of empty CPMV capsids can be achieved via mild alkaline hydrolysis of the viral RNA [71].

The majority of research on viruses has focused on their roles as infectious agents, however viruses are now being used in novel materials [72,73], in electrode applications [74], as nanoreactors for enzymatic processes [75] and as delivery agents for therapeutics [76] or contrast generating materials [77]. The shells of viruses without nucleic acid inside are known as capsids. For many viruses the capsid form is stable so they can be used without causing infection and it is these non-infectious forms that are used as contrast agents. Viruses may be modified to carry contrast within their cavity, at the interface of their subunits and on their outer faces (Figure 4D). We will discuss the virus-based contrast agents reported below, focusing first on viruses modified with small molecules or ions, then on viruses modified with inorganic nanoparticles.

### 3.1 Small molecule/ion modified viruses

The first virus to be adapted as an MRI contrast agent was the cowpea chlorotic mottle virus (CCMV) [78]. This virus has 180 metal binding sites between its protein subunits, which normally bind $Ca^{2+}$ ions. In this study, some of the $Ca^{2+}$ ions were replaced with $Gd^{3+}$ ions, producing a contrast agent of very high relaxivity (a measure of contrast agent efficacy), with an $r_1$ value of 202 $mM^{-1}s^{-1}$ at 60 MHz, which is almost 100-fold greater than that of commercial contrast agents. The binding of the gadolinium to the virus is rather weak, however, and therefore Gd-CCMV could have issues with transmetallation and toxicity. Anderson et al conjugated the commonly used chelate, DTPA, to the coat of the MS2 bacteriophage, creating a contrast agent that binds gadolinium strongly and has a relaxivity of 14.0 $mM^{-1}s^{-1}$, in the typical range of gadolinium-labeled nanoparticles [79]. Subsequently, the DOTA and HOPO gadolinium chelates have also been appended to viruses [80,81]. The pharmacokinetics and biodistribution of Gd-DOTA modified cowpea mosaic viruses (Gd-CPMV) have been investigated in mice [82]. At the dose used, Gd-CPMV cleared from the bloodstream within 20 minutes of injection and, at 30 minutes, the majority of the injected dose had gathered in the liver, with a small amount in the spleen. The behavior of the mice was normal post-injection and histological examination of the organs revealed no necrosis or tissue degeneration. Overall, it seems that these virus constructs are biocompatible, at least in the short term. Gd-CCMV additionally labeled with fluorescein, a fluorophore, and targeted to bacteria with an antibody

has been reported [83]. This contrast agent was shown to bind to the target bacteria with TEM and confocal microscopy.

Sherry and co-workers modified the surface of adenoviruses with thulium-DOTA complexes [84]. They found that the ability of the virus to transfect luciferase was maintained up until 800–900 DOTA chelates were attached to the surface of each viral capsid. The transfection ability dropped precipitously when the number of chelates increased above 900. Thulium allows contrast to be induced for MRI using a scanning sequence known as PARACEST, and when PARACEST was applied a change in signal intensity of 12% in images of solutions of thulium-labeled adenoviruses was produced.

Two reports were published in 2008 where viruses were labeled with $^{18}$F, a nucleus that decays to emit a positron, providing contrast for PET. The group of Francis selectively modified the interior of MS2 bacteriophages with [$^{18}$F]fluorobenzaldehyde ($^{18}$F-MS2) via a reaction with tyrosine residues, which are only expressed on the inner surface of the virus capsid [85]. PET imaging of rats was carried out post-injection with $^{18}$F-MS2. The agent was observed to localize in the liver, whereas [$^{18}$F]fluorobenzaldehyde transferred from the kidneys to the bladder. Further PET imaging experiments showed that loading the inner compartment of the virus with a therapeutic, coumarin, did not alter its distribution. The second report detailed the loading of hemagglutinating virus of Japan capsids with iron oxides and F-18 fluoride ions simultaneously [86] and also showed this virus-based PET tracer to gather in the liver of rats, post-injection.

Furthermore, viruses have been modified with a variety of fluorophores to act as contrast agents for fluorescent imaging [87]. Lewis et al conjugated Alexa 555, Alexa 488 or fluorescein to CPMV and found these fluorescent virus nanoparticles useful for the visualization of blood vessels in intravital microscopy. These agents were additionally applied to image new blood vessels forming in tumors.

### 3.2 Inorganic nanoparticle modified viruses

The technology of modification of viruses with inorganic nanoparticles such as iron oxide, gold nanoparticles and quantum dots, is quite advanced, with numerous reports in the literature [72,73,88–90]. Joo et al labeled the surface of HIV with quantum dots using a biotin-strepavidin linkage, which allowed live cell imaging of the trafficking of this virus into endosomal compartments [91]. In a 2007 report, adenoviruses were modified with manganese iron oxide (MnMEIO), as depicted schematically in ure 5A and in TEM images in Figure 5B. U251N cells, which highly express receptors for adenoviruses were incubated with adenovirus-MnMEIO nanoparticles. MR images of these cells revealed much greater signal loss, and hence particle uptake, than untreated U251N cells, U251N cells incubated with MnMEIO and CHO-1 cells, which have low expression of receptors for adenoviruses, incubated with adenovirus-MnMEIO (Figure 5C). Furthermore, the ability of adenovirus-MnMEIO nanoparticles to transfect the cells was maintained, as demonstrated by fluorescence imaging of cells transfected with GFP (Figure 5D-F).

## 4 Ferritin

Iron is stored and managed in the body by a nanoparticle called ferritin, which is composed of 1 nm thick, 24 subunit (ca. 20 kilodaltons each) protein coating known as apoferritin, which surrounds a 10 nm hydrated iron oxide core ($FeO_2H$) that includes around 4500 iron atoms [92]. Iron entering the body reacts with apoferritin to form ferritin, where it is stored until required by cell constituents such as cytochromes, nitrogenase, hemoglobin and so forth. The amino acid sequence of ferritin varies quite substantially between organisms, but also between the different organs of the same organism. Iron regulation is an important function and so

ferritin is found in every cell of mammals. The level of ferritin in patients is a marker for diseases such as anemia, porphyria and hemochromatosis.

As ferritin possesses an iron oxide core it is possible that this nanoparticle can generate contrast for MRI. Endogenous levels of ferritin can indeed be detected by the correct MR sequence, most commonly in the brain, where it has been used to study lesions in the brains of Parkinson's patients [93]. More recently, ferritin has been detected in the atherosclerotic plaques of rabbits [94] and when produced by a gene transfected to overexpress ferritin in mice [95]. The relaxometric properties of ferritin have been extensively investigated *in vitro* [96–98]. Meade and co-workers have reported ferritin bound to liposomes, whose relaxivity was higher than that of free ferritin due to the aggregation of ferritin at the liposome surface [99]. Iron oxide particles synthesized within the cavity of apoferritin have been applied for the imaging of macrophages [100]. Bennett et al compared normal ferritin (NF) and cationized ferritin (CF) for the detection of basement membranes, matrices of proteins and proteoglycans that support epithelial and endothelial cells [101]. There is a thick, negatively charged basement membrane in the glomeruli of the kidneys, therefore it was hypothesized that CF would be superior for detecting glomeruli. The basement membrane breaks down in renal diseases [102] and thus a method for non-invasively detecting its structure would be very valuable. The authors found CF to produce a speckled pattern of signal loss through the kidney of normal rats, when imaged 1.5 hours after injection, whereas there was little accumulation of NF (Figure 6A and B). Confocal microscopy performed on sections of kidney stained for ferritin confirmed that CF accumulated in glomeruli (Figure 6C and D). A rat disease model of focal and segmental glomerulosclerosis (FSGS) was used in the study and images of the kidneys of normal, early stage FSGS and late stage FSGS rats treated with CF are compared in Figure 6E-G. As the disease progressed, the pattern of ferritin deposition in the kidney changed from speckled to more and more diffuse, a result which is consistent with loss of glomerular integrity and permeation of large proteins through the glomerulus in such diseases.

Alternatively, the iron oxide core of ferritin has been replaced with a variety of materials such as uranium [103], platinum anti-cancer drugs [104] and quantum dots [105]. Aime et al reported the loading of apoferritin with gadolinium chelates via disassembling the protein subunits by lowering the pH to 2, before adding Gd-HPDO3A and raising the pH to 7 [106]. At pH=7 the protein subunits reassembled, trapping Gd-HPDO3A in the nanoparticle cavity (Figure 7A). Biotin moieties were added to the protein subunits leading to a particle (Gd-ferritin) that could be targeted via incubation with streptavidin and biotinylated C3d peptides, which are specific for receptors on vascular cells [107]. This nanoparticle was shown to be effective for MR imaging of tumor blood vessels in a mouse model of cancer, with significantly greater contrast produced in the tumor with C3d targeted Gd-ferritin than untargeted Gd-ferritin (Figure 7B-D).

## 5 Discussion

We have discussed examples of natural nanoparticle contrast agents for most of the available imaging techniques. These nanoparticles can deliver contrast generating materials to their natural targets or be re-routed to other receptors by the conjugation of targeting ligands. Natural nanoparticles have the advantage that they can be synthesized with quite precise size control, are potentially non-immunogenic and biodegradable. Modifying natural nanoparticles as contrast agents may also yield routes to novel materials and greater knowledge of the chemistry of these important endogenous nanoparticles.

With respect to the lipoproteins, HDL has some advantages over the other lipoproteins as it is atheroprotective rather than atherogenic and it is easier to reconstitute as the protein and phospholipids of HDL can be separated and subsequently reformed into particles whereas those

of the other lipoproteins cannot. In favor of the other lipoproteins, they can carry greater payloads of contrast generating materials. An issue that surrounds some contrast agents reported as being 'lipoprotein-based' is that the properties of the contrast agent differ very substantially from those of lipoproteins. The minimal criteria would be that, compared to the lipoprotein in question, the contrast agent has i) an average diameter in the relevant size range, ii) has a similar size distribution and iii) contains the correct apolipoprotein or an adequate substitute such as a peptide mimic.

As can be seen from the examples highlighted in this review, there are a large number of candidate viruses for adaptation as contrast agents. The available viruses have quite widely differing properties in terms of their availability, cells they target, dimensions and ways in which they can be modified [67], so the choice of virus is application dependant. As highlighted in section 3.1 above, the MS2 capsid is notable because the interior can be selectively modified [85], which can be very attractive. A notable problem with virus-based delivery systems is toxicity and immune responses [108]. This is being ameliorated by use of polymer coatings added to the virus exteriors [109].

The eventual goal of developing modified natural nanoparticle contrast agents is to use them in patients for diagnosis, to discover more about human diseases or the effects of treatment. Before meeting this goal there are several important challenges that need to be overcome. First is to develop methods to ensure no contamination of naturally derived contrast agents with pathogens or, in the case of viruses, infectious forms of the contrast agent. Another challenge would be creating synthesis procedures for widespread use of these agents. Lipoproteins can be extracted from expired human plasma or from the patients themselves. Some viruses can be produced in culture in large quantities. For translation to the clinic, these agents will need to be demonstrated safe (i.e. of insignificant toxicity) and effective *in vivo* in clinical scanners prior to human trials. Standardized, validated natural nanoparticle contrast agents could also be very valuable for disease investigations in pre-clinical research. Looking to the future, we expect work on these goals to proceed, as well as applications of more novel natural nanoparticle contrast agents to be reported revealing valuable information on biological processes.

## Acknowledgments

Partial support was provided by: NIH/NHLBI ROI HL71021, NIH/NHLBI HL78667 (ZAF).

## References

1. Lauterbur PC. Image Formation by Induced Local Interactions: Examples Employing Nuclear Magnetic Resonance. Nature 1973;242:190–191.
2. Hounsfield GN. Computerized transverse axial scanning (tomography): Part I. Description of system. Brit J Radiol 1973;46:1016–1022. [PubMed: 4757352]
3. Basser PJ, Mattiello J, LeBihan D. MR diffusion tensor spectroscopy and imaging. Biophys J 1994;66:259–267. [PubMed: 8130344]
4. Rudd JHF, Warburton EA, Fryer TD, Jones HA, Clark JC, Antoun N, Johnstrom P, Davenport AP, Kirkpatrick PJ, Arch BN, Pickard JD, Weissberg PL. Imaging atherosclerotic plaque inflammation with [F-18]-fluorodeoxyglucose positron emission tomography. Circulation 2002;105:2708–2711. [PubMed: 12057982]
5. Padhani AR. Dynamic contrast-enhanced MRI in clinical oncology: Current status and future directions. J Mag Reson Imaging 2002;16:407–422.
6. Calcagno C, Cornily JC, Hyafil F, Rudd JHF, Briley-Saebo KC, Mani V, Goldschlager G, Machac J, Fuster V, Fayad ZA. Detection of neovessels in atherosclerotic plaques of rabbits using dynamic contrast enhanced MRI and 18F-FDG PET. Arterioscler Thromb Vasc Biol 2008;28:1311–1317. [PubMed: 18467641]

7. Mulder WJM, Griffioen AW, Strijkers GJ, Cormode DP, Nicolay K, Fayad ZA. Magnetic and fluorescent nanoparticles for multimodality imaging. Nanomedicine 2007;2:307–324. [PubMed: 17716176]
8. Corot C, Robert P, Idee JM, Port M. Recent advances in iron oxide nanocrystal technology for medical imaging. Adv Drug Deliv Rev 2006;58:1471–1504. [PubMed: 17116343]
9. Azzazy HME, Mansour MMH, Kazmierczak SC. From diagnostics to therapy: Prospects of quantum dots. Clin Biochem 2007;40:917–927. [PubMed: 17689518]
10. Huang X, El-Sayed IH, Qian W, El-Sayed MA. Cancer cell imaging and photothermal therapy in the near-infrared region by using gold nanorods. J Am Chem Soc 2006;128:2115–2120. [PubMed: 16464114]
11. Bulte JWM, Kraitchman DL. Iron oxide MR contrast agents for molecular and cellular imaging. NMR Biomed 2004;17:484–499. [PubMed: 15526347]
12. Smith AM, Duan H, Mohs AM, Nie S. Bioconjugated quantum dots for in vivo molecular and cellular imaging. Adv Drug Deliv Rev 2008;60:1226–1240. [PubMed: 18495291]
13. Cormode DP, Skajaa T, Fayad ZA, Mulder WJM. Nanotechnology in medical imaging: probe design and applications, Arterioscler. Thromb Vasc Biol. 2009 in press.
14. Mulder WJM, Strijkers GJ, van Tilborg GAF, Griffioen AW, Nicolay K. Lipid-based nanoparticles for contrast-enhanced MRI and molecular imaging. NMR in Biomedicine 2006;19:142–164. [PubMed: 16450332]
15. McCarthy JR, Kelly KA, Sun EY, Weissleder R. Targeted delivery of multifunctional magnetic nanoparticles. Nanomedicine 2007;2:153–167. [PubMed: 17716118]
16. Medintz IL, Uyeda HT, Goldman ER, Mattoussi H. Quantum dot bioconjugates for imaging, labelling and sensing. Nat Mater 2005;4:435–446. [PubMed: 15928695]
17. Kim D, Park S, Lee JH, Jeong YY, Jon S. Antibiofouling polymer-coated gold nanoparticles as a contrast agent for in vivo x-ray computed tomography imaging. J Am Chem Soc 2007;129:7661–7665. [PubMed: 17530850]
18. Cormode DP, Skajaa T, van Schooneveld MM, Koole R, Jarzyna P, Lobatto ME, Calcagno C, Barazza A, Gordon RE, Zanzonico P, Fisher EA, Fayad ZA, Mulder WJM. Nanocrystal core high-density lipoproteins: A multimodal molecular imaging contrast agent platform. Nano Lett 2008;8:3715–3723. [PubMed: 18939808]
19. Rabin O, Perez JM, Grimm J, Wojtkiewicz G, Weissleder R. An X-ray computed tomography imaging agent based on long-circulating bismuth sulphide nanoparticles. Nat Mater 2006;5:118–122. [PubMed: 16444262]
20. Hyafil F, Cornily JC, Feig JE, Gordon R, Vucic E, Amirbekian V, Fisher EA, Fuster V, Feldman LJ, Fayad ZA. Noninvasive detection of macrophages using a nanoparticulate contrast agent for computed tomography. Nat Med 2007;13:636–641. [PubMed: 17417649]
21. Mukundan S, Ghaghada KB, Badea CT, Kao CY, Hedlund LW, Provanzale JM, Johnson GA, Chen E, Bellamkonda RV, Annapragada A. A liposomal nanoscale contrast agent for preclinical CT in mice. Am J Roentgenol 2006;186:300–307. [PubMed: 16423931]
22. Amirbekian V, Lipinski MJ, Briley-Saebo KC, Amirbekian S, Aguinaldo JG, Weinreb DB, Vucic E, Frias JC, Hyafil F, Mani V, Fisher EA, Fayad ZA. Detecting and assessing macrophages in vivo to evaluate atherosclerosis noninvasively using molecular MRI. Proc Natl Acad Sci USA 2007;104:961–966. [PubMed: 17215360]
23. Mulder WJM, Strijkers GJ, Griffioen AW, van Bloois L, Molema G, Storm G, Koning GA, Nicolay K. A liposomal system for contrast-enhanced magnetic resonance imaging of molecular targets. Bioconjugate Chem 2004;15:799–806.
24. Lanza GM, Winter PM, Caruthers SD, Hughes MS, Cyrus T, Marsh JN, Neubauer AM, Partlow KC, Wickline SA. Nanomedicine opportunities for cardiovascular disease with perfluorocarbon nanoparticles. Nanomedicine 2006;1:321–329. [PubMed: 17716162]
25. van Schooneveld MM, Vucic E, Koole R, Zhou Y, Stocks J, Cormode DP, Tang CY, Gordon R, Nicolay K, Meijerink A, Fayad ZA, Mulder WJM. Improved biocompatibility and pharmacokinetics of silica nanoparticles by means of a lipid coating: a multimodality investigation. Nano Lett 2008;8:2517–2525. [PubMed: 18624389]

26. Sitharaman B, Kissell KR, Hartman KB, Tran LA, Baikalov A, Rusakova I, Sun Y, Khant HA, Ludtke SJ, Chiu W, Laus S, Toth W, Helm L, Merbach AE. Superparamagnetic gadonanotubes are high-performance MRI contrast agents. Chem Commun 2005:3915–3917.
27. Klibanov AL, Maruyama K, Torchilin VP, Huang L. Amphipatic polyethyleneglycols effectively prolong the circulation time of liposomes. FEBS Lett 1990;268:235–238. [PubMed: 2384160]
28. Mulder WJM, Koole R, Brandwijk RJ, Storm G, Chin PTK, Strijkers GJ, Donega CD, Nicolay K, Griffioen AW. Quantum dots with a paramagnetic coating as a bimodal molecular imaging probe. Nano Lett 2006;6:1–6. [PubMed: 16402777]
29. Reimer P, Tombach B. Hepatic MRI with SPIO: detection and characterization of focal liver lesions. European Radiology 1998;8:1198–1204. [PubMed: 9724439]
30. Zhang Z, Greenfield MT, Spiller M, McMurry TJ, Lauffer RB, Caravan P. Multilocus binding increases the relaxivity of protein-bound MRI contrast agents. Angew Chem Int Ed 2005;44:6766–6769.
31. de Vries IJM, Lesterhuis WJ, Barentsz JO, Verdijk P, van Krieken JH, Boerman OC, Oyen WJG, Bonenkamp JJ, Boezeman JB, Adema GJ, Bulte JWM, Scheenen TWJ, Punt CJA, Heerschap A, Figdor CG. Magnetic resonance tracking of dendritic cells in melanoma patients for monitoring of cellular therapy. Nat Biotech 2005;23:1407–1413.
32. Havel RJ, Eder HA, Bragdon JH. The distribution and chemical composition of ultracentrifugally separated lipoproteins in human serum. J Clin Invest 1955;34:1345–1353. [PubMed: 13252080]
33. Wasan KM, Brocks DR, Lee SD, Sachs-Barrable K, Thornton SJ. Impact of lipoproteins on the biological activity and disposition of hydrophobic drugs: implications for drug discovery. Nat Rev Drug Discov 2008;7:84–99. [PubMed: 18079757]
34. Nichols AV, Krauss RM, Musliner TA. Nondenaturing polyacrylamide gradient gel electrophoresis. Method Enzymol 1986;128:417–431.
35. Acton S, Rigotti A, Landschulz KT, Xu S, Hobbs HH, Kriegert M. Identification of scavenger receptor SR-BI as a high density lipoprotein receptor. Science 1996;271:518–520. [PubMed: 8560269]
36. Davidson WS, Lund-Katz S, Johnson WJ, Anantharamaiah GM, Palgunachari MN, Segrest JP, Rothblat GH, Phillips MC. The influence of apolipoprotein structure on the efflux of cellular free cholesterol to high density lipoprotein. J Biol Chem 1994;269:22975–22982. [PubMed: 8083197]
37. Rye KA, Barter PJ. Antiinflammatory actions of HDL: a new insight. Arterioscler Thromb Vasc Biol 2008;28:1890–1891. [PubMed: 18946054]
38. Lusis AJ. Atherosclerosis. Nature 2000;407:233–241. [PubMed: 11001066]
39. Gordon DJ, Rifkind BM. High-density lipoprotein - the clinical implications of recent studies. New Eng J Med 1989;321:1311–1316. [PubMed: 2677733]
40. Shepherd J, Cobbe SM, Ford I, Isles CG, Lorimer AR, Macfarlane PW, McKillop JH, Packard CJ. Prevention of coronary heart disease with pravastatin in men with hypercholesterolemia. New Eng J Med 1995;333:1301–1307. [PubMed: 7566020]
41. Kontush A, Guerin M, Chapman MJ. Spotlight on HDL-raising therapies: insights from the torcetrapib trials. Nat Clin Pract, Cardiovasc Med 2008;5:329–336. [PubMed: 18431367]
42. Geninatti Crich S, Lanzardo S, Alberti D, Belfiore S, Ciampa A, Giovenzana GB, Lovazzano C, Pagliarin R, Aime S. Magnetic resonance imaging detection of tumor cells by targeting low-density lipoprotein receptors with Gd-loaded low-density lipoprotein particles. Neoplasia 2007;9:1046–1056. [PubMed: 18084612]
43. Sinzinger H, Bergmann H, Kaliman J, Angelberger P. Imaging of human atherosclerosis lesions using I-123 low-density-lipoprotein. Eur J Nucl Med 1986;12:291–292. [PubMed: 3780773]
44. Frias JC, Williams KJ, Fisher EA, Fayad ZA. Recombinant HDL-like nanoparticles: a specific contrast agent for MRI of atherosclerotic plaques. J Am Chem Soc 2004;126:16316–16317. [PubMed: 15600321]
45. Chen J, Corbin IR, Li H, Cao W, Glickson JD, Zheng G. Ligand conjugated low-density lipoprotein nanoparticles for enhanced optical cancer imaging in vivo. J Am Chem Soc 2007;129:5798–5799. [PubMed: 17428054]
46. McConathy WJ, Nair MP, Paranjape S, Mooberry L, Lacko AG. Evaluation of synthetic/reconstituted high-density lipoproteins as delivery vehicles for paclitaxel. Anti-cancer drugs 2008;19:183–188. [PubMed: 18176115]

47. Zheng G, Chen J, Li H, Glickson JD. Rerouting lipoprotein nanoparticles to selected alternate receptors for the targeted delivery of cancer diagnostic and therapeutic agents. Proc Natl Acad Sci USA 2005;102:17757–17762. [PubMed: 16306263]
48. Shaish A, Keren G, Chouraqui P, Levkovitz H, Harats D. Imaging of aortic atherosclerotic lesions by 125I-LDL, 125I-Oxidized-LDL, 125I-HDL and 125I-BSA. Pathobiology 2001;69:225–229. [PubMed: 12007282]
49. Nakashima Y, Plump AS, Raines EW, Breslow JL, Ross R. ApoE-deficient mice develop lesions of all phases of atherosclerosis through the arterial tree. Arterioscler Thromb 1994;14:133–140. [PubMed: 8274468]
50. Frias JC, Ma Y, Williams KJ, Fayad ZA, Fisher EA. Properties of a versatile nanoparticle platform contrast agent to image and characterize atherosclerotic plaques by magnetic resonance imaging. Nano Lett 2006;6:2220–2224. [PubMed: 17034087]
51. Jonas A. Reconstitution of high-density lipoproteins. Method Enzymol 1986;128:553–582.
52. Naghavi M, Libby P, Falk E, Casscells SW, Litovsky S, Rumberger J, Badimon JJ, Stefanadis C, Moreno P, Pasterkamp G, Fayad Z, Stone PH, Waxman S, Raggi P, Madjid M, Zarrabi A, Burke A, Yuan C, Fitzgerald PJ, Siscovick DS, de Korte CL, Aikawa M, Airaksinen KEJ, Assmann G, Becker CR, Chesebro JH, Farb A, Galis ZS, Jackson C, Jang IK, Koenig W, Lodder RA, March K, Demirovic J, Navab M, Priori SG, Rekhter MD, Bahr R, Grundy SM, Mehran R, Colombo A, Boerwinkle E, Ballantyne C, Insull W, Schwartz RS, Vogel R, Serruys PW, Hansson GK, Faxon DP, Kaul S, Drexler H, Greenland P, Muller JE, Virmani R, Ridker PM, Zipes DP, Shah PK, Willerson JT. From vulnerable plaque to vulnerable patient - A call for new definitions and risk assessment strategies: Part I. Circulation 2003;108:1664–1672. [PubMed: 14530185]
53. Briley-Saebo KC, Geninatti Crich S, Cormode DP, Barazza A, Mulder WJM, Chen W, Giovenzana GB, Fisher EA, Aime S, Fayad ZA. High-Relaxivity Gadolinium-Modified High-Density Lipoproteins as Magnetic Resonance Imaging Contrast Agents. J Phys Chem B. 2009 online.
54. Cormode DP, Briley-Saebo KC, Mulder WJM, Aguinaldo JGS, Barazza A, Ma Y, Fisher EA, Fayad ZA. An apoA-I mimetic peptide HDL-based MRI contrast agent for atherosclerotic plaque composition detection. Small 2008;4:1437–1444. [PubMed: 18712752]
55. Cormode DP, Chandrasekar R, Delshad A, Briley-Saebo KC, Calcagno C, Barazza A, Mulder WJM, Fisher EA, Fayad ZA. Comparison of synthetic HDL contrast agents for MR imaging of atherosclerosis. Bioconjugate Chem. 2009 in press.
56. Chen W, Vucic E, Leupold E, Mulder WJM, Cormode DP, Briley-Saebo KC, Barazza A, Fisher EA, Dathe M, Fayad ZA. Incorporation of an apoE-derived lipopeptide in high-density lipoprotein MRI contrast agents for enhanced imaging of macrophages in atherosclerosis. Contrast Media Mol Imaging 2008;3:233–242. [PubMed: 19072768]
57. Sauer I, Nikolenko H, Keller S, Abu Ajaj K, Blenert M, Dathe M. Dipalmitoylation of a cellular uptake-mediating apolipoprotein E-derived peptide as a promising modification for stable anchorage in liposomal drug carriers. Biochim Biophys Acta Biomemb 2006;1758:552–561.
58. Rosen JM, Butler SP, Meinken GE, Wang TST, Ramakrishnan R, Srivastava SC, Alderson PO, Ginsberg HN. Indium-111-labeled LDL: a potential agent for imaging atherosclerotic disease and lipoprotein biodistribution. J Nucl Med 1990;31:343–350. [PubMed: 2308006]
59. Pietzsch J, Bergmann R, Rode K, Hultsch C, Pawelke B, Wuest F, van den Hoff J. Fluorine-18 radiolabeling of low-density lipoproteins: a potential approach for characterization and differentiation of metabolism of native and oxidized low-density lipoproteins in vivo. Nucl Med Biol 2004;31:1043–1050. [PubMed: 15607486]
60. Ginsberg HN, Goldsmith SJ, Vallabajosula S. Noninvasive imaging of 99mTechnetium-labeled low density lipoprotein uptake by tendon xanthomas in hypercholesterolemic patients. Arteriosclerosis 1990;10:256–262. [PubMed: 2317159]
61. Corbin IR, Li H, Chen J, Lund-Katz S, Zhou R, Glickson JD, Zheng G. Low-density lipoprotein nanoparticles as magnetic resonance imaging contrast agents. Neoplasia 2006;8:488–498. [PubMed: 16820095]
62. Mitsumori LM, Ricks JL, Rosenfeld ME, Schmiedl UP, Yuan C. Development of a lipoprotein based molecular imaging MR contrast agent for the noninvasive detection of early atherosclerotic disease. Int J Cardiovasc Imaging 2004;20:561–567. [PubMed: 15856643]

63. Li H, Gray BD, Corbin IR, Lebherz C, Choi H, Lund-Katz S, Wilson JM, Glickson JD, Zhou R. MR and fluorescent imaging of low-density lipoprotein receptors. Acad Radiol 2004;11:1251–1259. [PubMed: 15561572]
64. Huettinger M, Corbett JR, Schneider WJ, Willerson JT, Brown MS, Goldstein JL. Imaging of hepatic low-density lipoprotein receptors by radionuclide scintiscanning in vivo. Proc Nat Acad Sci USA 1984;81:7599–7603. [PubMed: 6594702]
65. Longino MA, Bakan DA, Weichert JP, Counsell RE. Formulation of polyiodinated triglyceride analogues in a chylomicron remnant-like liver-selective delivery vehicle. Pharm Res 1996;13:875–879. [PubMed: 8792425]
66. Wisner ER, Weichert JP, Longino MA, Counsell RE, Weisbrode SE. A surface-modified chylomicron remnant-like emulsion for percutaneous computed tomography lymphography. Invest Radiol 2002;37:232–239. [PubMed: 11923646]
67. Douglas T, Young M. Viruses: making friends with old foes. Science 2006;312:873–875. [PubMed: 16690856]
68. Suttle CA. Viruses in the sea. Nature 2005;437:356–361. [PubMed: 16163346]
69. Johnson J, Lin T, Lomonossoff G. Presentation of heterologous peptides on plant viruses: genetics, structure, and function. Annu Rev Phytopathol 1997;35:67–86. [PubMed: 15012515]
70. Wellink, J. Comovirus isolation and RNA extraction. In: Foster, GD.; Taylor, SC., editors. Plant virology protocols: from virus isolation to transgene resistance. Humana Press; Totana, New Jersey: 1998. p. 205-209.
71. Ochoa WF, Chatterji A, Lin TW, Johnson JE. Generation and structural analysis of reactive empty particles derived from an icosahedral virus. Chemistry & Biology 2006;13:771–778. [PubMed: 16873025]
72. Royston E, Lee SY, Culver JN, Harris MT. Characterization of silica-coated tobacco mosaic virus. J Coll Interf Sci 2006;298:706–712.
73. Dujardin E, Peet C, Stubbs G, Culver JN, Mann S. Organization of metallic nanoparticles using tobacco mosaic virus templates. Nano Lett 2003;3:413–417.
74. Nam KT, Wartena R, Yoo PJ, Liau FW, Lee YJ, Chiang YM, Hammond PT, Belcher AM. Stamped microbattery electrodes based on self-assembled M13 viruses. Proc Natl Acad Sci USA 2008;105:17227–17231. [PubMed: 18753629]
75. Comellas-Aragones M, Engelkamp H, Claessen VI, Sommerdijk NAJM, Rowan AE, Christianen PCM, Maan JC, Verduin BJM, Cornelissen JJLM, Nolte RJM. A virus-based single-enzyme nanoreactor. Nat Nano 2007;2:635–639.
76. Flenniken ML, Liepold LO, Crowley BE, Willits DA, Young M, Douglas T. Selective attachment and release of a chemotherapeutic agent from the interior of a protein cage architecture. Chem Commun 2005:447–449.
77. Huh YM, Lee ES, Lee JH, Jun YW, Kim PH, Yun CO, Kim JH, Suh JS, Cheon J. Hybrid nanoparticles for magnetic resonance imaging of target-specific viral gene delivery. Adv Mater 2007;19:3109–3112.
78. Allen M, Bulte JWM, Liepold L, Basu G, Zywicke HA, Frank JA, Young M, Douglas T. Paramagnetic viral nanoparticles as potential high-relaxivity magnetic resonance contrast agents. Magn Reson Med 2005;54:807–812. [PubMed: 16155869]
79. Anderson EA, Isaacman S, Peadbody DS, Wang EY, Canary JW, Kirshenbaum K. Viral nanoparticles donning a paramagnetic coat: conjugation of MRI contrast agents to the MS2 capsid. Nano Lett 2006;6:1160–1164. [PubMed: 16771573]
80. Datta A, Hooker JM, Botta M, Francis MB, Aime S, Raymond KN. High relaxivity gadolinium hydroxypyridonate viral capsid conjugates: nanosized MRI contrast agents. J Am Chem Soc 2008;130:2546–2552. [PubMed: 18247608]
81. Liepold L, Anderson S, Willits DA, Oltrogge L, Frank JA, Douglas T, Young M. Viral capsids as MRI contrast agents. Magn Reson Med 2007;58:871–879. [PubMed: 17969126]
82. Singh P, Prasuhn D, Yeh RM, Destito G, Rae CS, Osburn K, Finn MG, Manchester M. Bio-distribution, toxicity and pathology of cowpea mosaic virus nanoparticles in vivo. J Control Release 2007;120:41–50. [PubMed: 17512998]

83. Suci PA, Berglund DL, Liepold L, Brumfield S, Pitts B, Davison W, Oltrogge L, Hoyt KO, Codd S, Stewart PS, Young M, Douglas T. High-density targeting of a viral multifunctional nanoplatform to a pathogenic, biofilm-forming bacterium. Chem Biol 2007;14:387–398. [PubMed: 17462574]
84. Vasalatiy O, Gerard RD, Zhao P, Sun X, Sherry AD. Labeling of adenovirus particles with PARACEST agents. Bioconjugate Chem 2008;19:598–606.
85. Hooker JM, O'Neil JP, Romanini DW, Taylor SE, Francis MB. Genome-free viral capsids as carriers for positron emission tomography radiolabels. Mol Imaging Biol 2008;10:182–191. [PubMed: 18437498]
86. Flexman JA, Cross DJ, Lewellen BL, Miyoshi S, Kim Y, Minoshima S. Magnetically targeted viral envelopes: a PET investigation of initial biodistribution. IEEE Trans Nanobiosci 2008;7:223–232.
87. Lewis JD, Destito G, Zijlstra A, Gonzalez MJ, Quigley JP, Manchester M, Stuhlmann H. Viral nanoparticles as tools for intravital vascular imaging. Nat Med 2006;12:354–360. [PubMed: 16501571]
88. Chen C, Daniel MC, Quinkert ZT, De M, Stein B, Bowman VD, Chipman PR, Rotello VM, Kao CC, Dragnea B. Nanoparticle-templated assembly of viral protein cages. Nano Lett 2006;6:611–615. [PubMed: 16608253]
89. Huang X, Bronstein LM, Retrum J, DuFort C, Tsvetkova I, Aniagyei S, Stein B, Stucky G, McKenna B, Remmes N, Baxter D, Kao CC, Dragnea B. Self-assembled virus-like particles with magnetic cores. Nano Lett 2007;7:2407–2416. [PubMed: 17630812]
90. Portney NG, Singh K, Chaudhary S, Destito G, Schneemann A, Manchester M, Ozkan M. Organic and inorganic nanoparticle hybrids. Langmuir 2005;21:2098–2103. [PubMed: 15751992]
91. Joo KI, Lei Y, Lee CH, Lo J, Xie J, Hamm-Alvarez SF, Wang P. Site-specific labeling of enveloped viruses with quantum dots for single virus tracking. ACS Nano 2008;2:1553–1562. [PubMed: 19079775]
92. Theil EC. Ferritin: structure, gene regulation, and cellular function in animals, plants and microorganisms. Ann Rev Biochem 1987;56:289–315. [PubMed: 3304136]
93. Gorell JM, Ordidge RJ, Brown GG, Deniau JC, Buderer NM, Helpern JA. Increased iron-related MRI contrast in the substantia-nigra in Parkinson's disease. Neurology 1995;45:1138–1143. [PubMed: 7783878]
94. Mani V, Briley-Saebo KC, Hyafil F, Fayad ZA. Feasibility of in vivo identification of endogenous ferritin with positive contrast MRI in rabbit carotid crush injury using GRASP. Magn Reson Med 2006;56:1096–1106. [PubMed: 17036302]
95. Genove G, DeMarco U, Xu H, Goins WF, Ahrens ET. A new transgene reporter for in vivo magnetic resonance imaging. Nat Med 2005;11:450–454. [PubMed: 15778721]
96. Brooks RA, Vymazal J, Goldfarb RB, Bulte JWM, Aisen P. Relaxometry and magnetometry of ferritin. Magn Reson Med 1998;40:227–235. [PubMed: 9702704]
97. Goussin Y, Gillis P, Muller RN, Hocq A. Relaxation by clustered ferritin: a model for ferritin-induced relaxation in vivo. NMR Biomed 2007;20:749–756. [PubMed: 17330925]
98. Bennett KM, Shapiro EM, Sotak CH, Koretsky AP. Controlled aggregation of ferritin to modulate MRI relaxivity. Biophys J 2008;95:342–351. [PubMed: 18326661]
99. Wood JC, Fassler JD, Meade T. Mimicking liver iron overload using liposomal ferritin preparations. Magn Reson Med 2004;51:607–611. [PubMed: 15004804]
100. Uchida M, Terashima M, Cunningham CH, Suzuki Y, Willits DA, Willis AF, Yang PC, Tsao PS, McConnell MV, Young MJ, Douglas T. A human ferritin iron oxide nano-composite magnetic resonance contrast agent. Magn Reson Med 2008;60:1073–1081. [PubMed: 18956458]
101. Bennett KM, Zhou H, Sumner JP, Dodd SJ, Bouraoud N, Doi K, Star RA, Koretsky AP. MRI of the basement membrane using charged nanoparticles as contrast agents. Magn Reson Med 2008;60:564–574. [PubMed: 18727041]
102. Russo LM, Sandoval RM, McKee M, Osicka TM, Collins AB, Brown D, Molitoris BA, Comper WD. The normal kidney filters nephrotic levels of albumin retrieved by proximal tubule cells: Retrieval is disrupted in nephrotic states. Kidney Int 2007;71:504–513. [PubMed: 17228368]
103. Hainfeld JF. Uranium-loaded apoferrin with antibodies attached: Molecular design for uranium neutron-capture therapy. Proc Natl Acad Sci 1992;89:11064–11064. [PubMed: 1438316]

104. Yang Z, Wang X, Diao H, Zhang J, Li H, Sun H, Guo Z. Encapsulation of platinum anticancer drugs by apoferritin. Chem Comm 2007:3453–3455. [PubMed: 17700879]

105. Hennequin B, Turyanska L, Ben T, Beltran AM, Molina SI, Li M, Mann S, Patane A, Thomas NR. Aqueous near-infrared fluorescent composites based on apoferritin-encapsulated PbS quantum dots. Adv Mater 2008;20:3592–3596.

106. Aime S, Frullano L, Geninatti Crich S. Compartmentalization of a gadolinium complex in the apoferritin cavity: a route to obtain high relaxivity contrast agents for magnetic resonance imaging. Angew Chem Int Ed 2002;41:1017–1019.

107. Geninatti Crich S, Bussolati B, Tei L, Grange C, Esposito G, Lanzardo S, Camussi G, Aime S. Magnetic resonance visualization of tumor angiogenesis by targeting neural cell adhesion molecules with the highly sensitive gadolinium-loaded apoferritin probe. Cancer Res 2006;66:9196–9201. [PubMed: 16982763]

108. Lorence RM, Roberts MS, O'Neil JD, Groene WS, Miller JA, Mueller SN, Bamat MK. Phase 1 clinical experience using intravenous administration of PV701, an oncolytic Newcastle disease virus. Curr Cancer Drug Targets 2007;7:157–167. [PubMed: 17346107]

109. Carlisle RC, Benjamin R, Briggs SS, Sumner-Jones S, McIntosh J, Gill D, Hyde S, Nathwani A, Subr V, Ulbrich K, Seymour LW, Fisher KD. Coating of adeno-associated virus with reactive polymers can ablate virus tropsim, enable retargeting and provide resistance to neutralising antisera. J Gene Med 2008;10:400–c 411. [PubMed: 18220318]

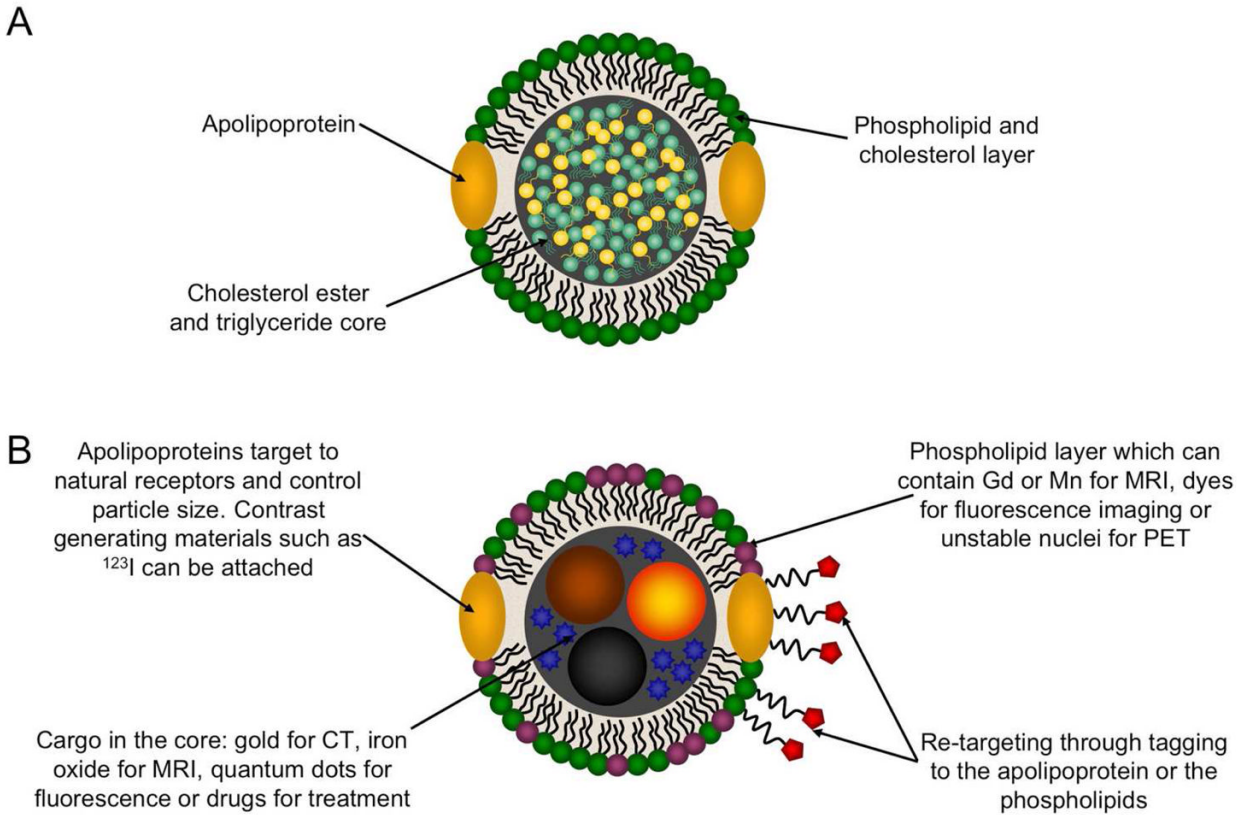


**Figure 1.**
A) Schematic depiction of lipoprotein structure. B) The ways in which lipoproteins may be modified to act as contrast agents.

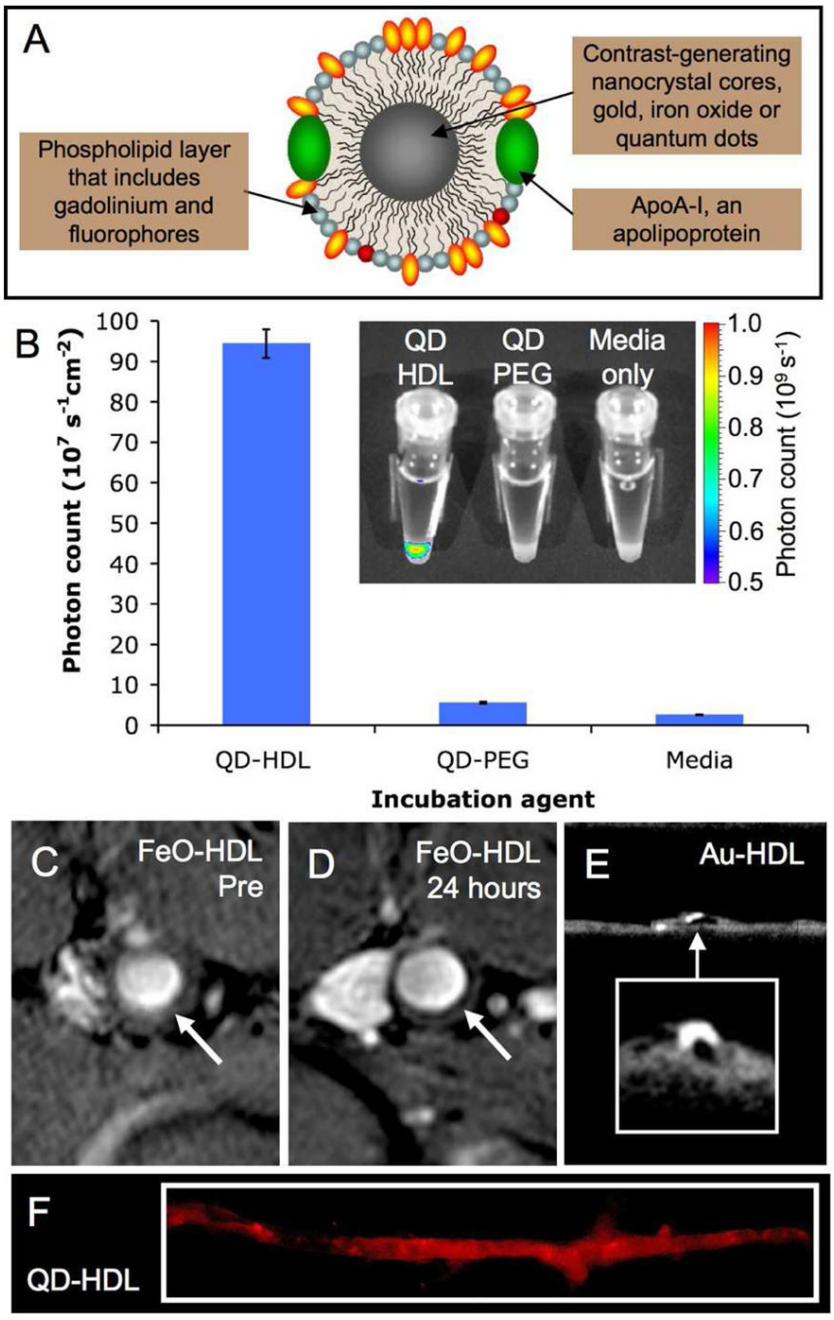


**Figure 2.**

A) Schematic of nanocrystal core HDL. B) QD-HDL was taken up preferentially by macrophage cells as evidenced by fluorescent imaging. FeOHDL produced negative contrast in the aorta of atherosclerotic mice when MR images taken C) pre-injection and D) 24 hours post-injection are compared. E) Micro-CT images of the excised aortas of mice showed significant uptake of Au-HDL. F) Fluorescent imaging showed QD-HDL to be taken up throughout the excised aorta of atherosclerotic mice. Figure adapted with permission from reference [18].

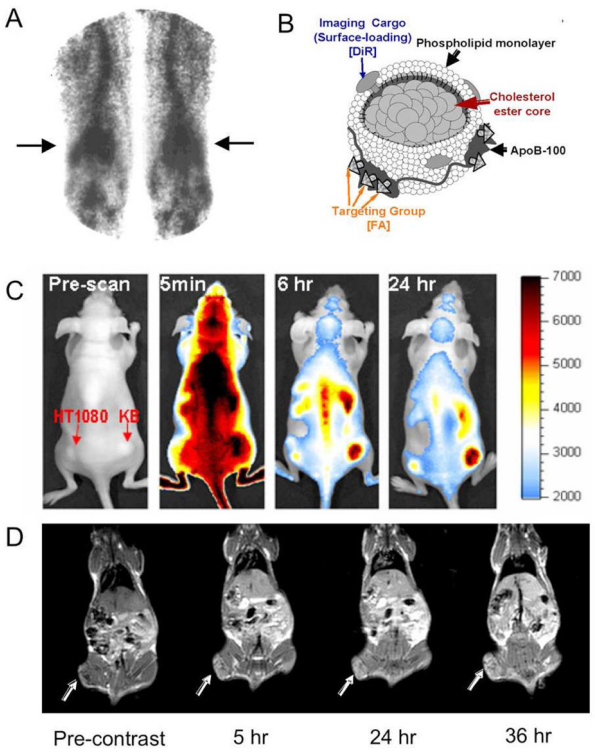


**Figure 3.**

A) A gamma camera image of the legs of a dyslipidemic patient injected with $^{99m}$Tc labeled LDL. The $^{99m}$Tc-LDL accumulated in lipid rich deposits at the knees known as xanthomas (arrows). B) Schematic depiction of LDL labeled with a fluorophore (DiR) and modified with folic acid (FA) to re-route the nanoparticle to the folate receptor (FA-LDL). C) Fluorescent images of a mouse inoculated with two tumors: a KB tumor, right, which highly expresses the folate receptor and a HT1080 tumor, left, which has low expression of the folate receptor. When FA-LDL was injected into the mouse, preferential accumulation of this contrast agent in the KB tumor occurred, indicating that the particle was successfully re-routed to the folate receptor. D) MR images of a mouse bearing a tumor (arrows) that highly expresses the LDL receptor pre-injection and 5, 24 and 36 hours post-injection with Gd-labeled LDL. The contrast produced in the tumor indicates that Gd-LDL can be used as a selective contrast agent for these tumors. The images in this figure are reproduced with permission from references [45,60,61].

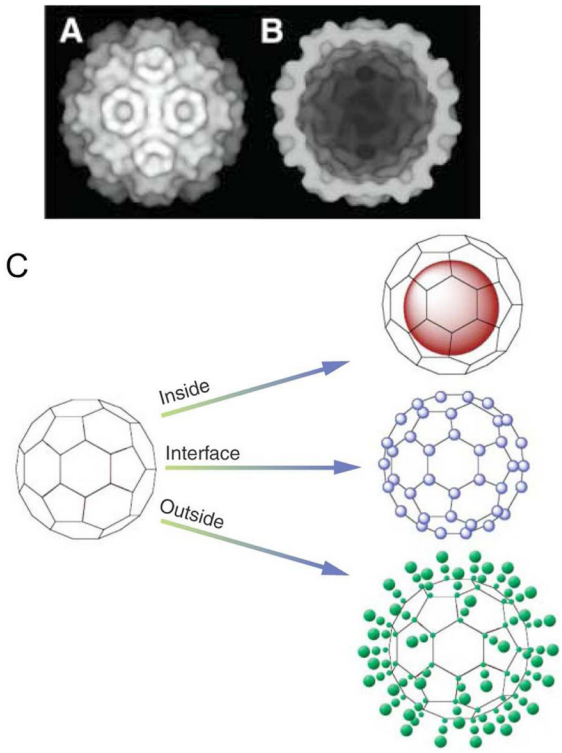


**Figure 4.**
A) Cryo–electron micrograph reconstruction of CCMV. B) Cut-through image of CCMV showing the interior cavity. C) Schematic of the three ways in which a virus particle can be loaded with contrast generating material: in the interior, at the interfaces between the subunits and on the exterior. Images reproduced, with permission, from reference [67].

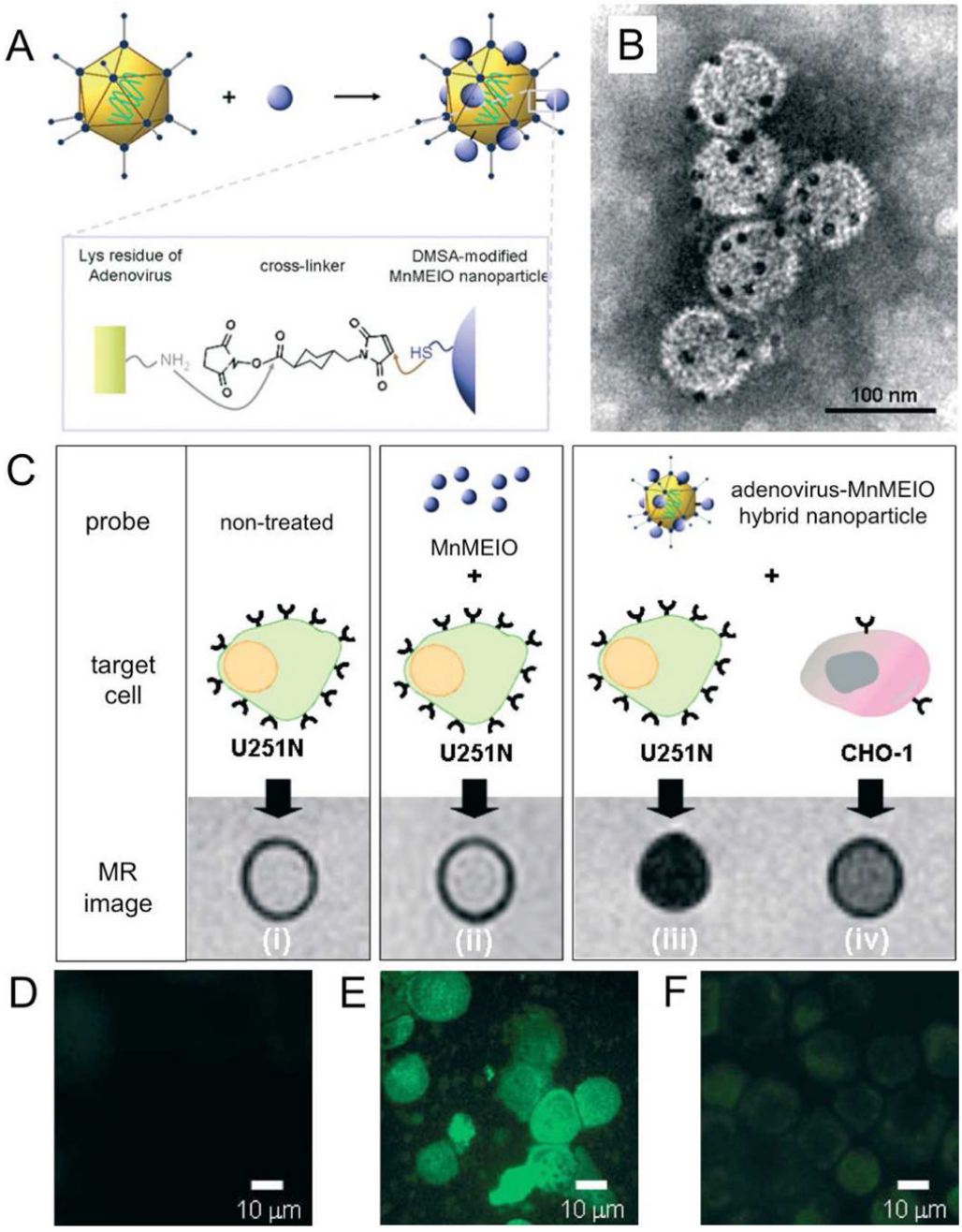


**Figure 5.**

A) Schematic depiction of the modification of adenoviruses with manganese iron oxide particles (MnMEIO). B) TEM image of the modified viruses, where the dark spots are the MnMEIO. C) T2-weighted MR images of U251N cells untreated, incubated with MnMEIO or adenovirus MnMEIO and CHO-1 cells incubated with adenovirus MnMEIO. Fluorescence images of D) untreated U251N cells, E) adenovirus MnMEIO treated U251N cells and F) adenovirus MnMEIO treated CHO-1 cells showing that the ability of the modified viruses to transfect cells is retained. Figure adapted with permission from reference [77].

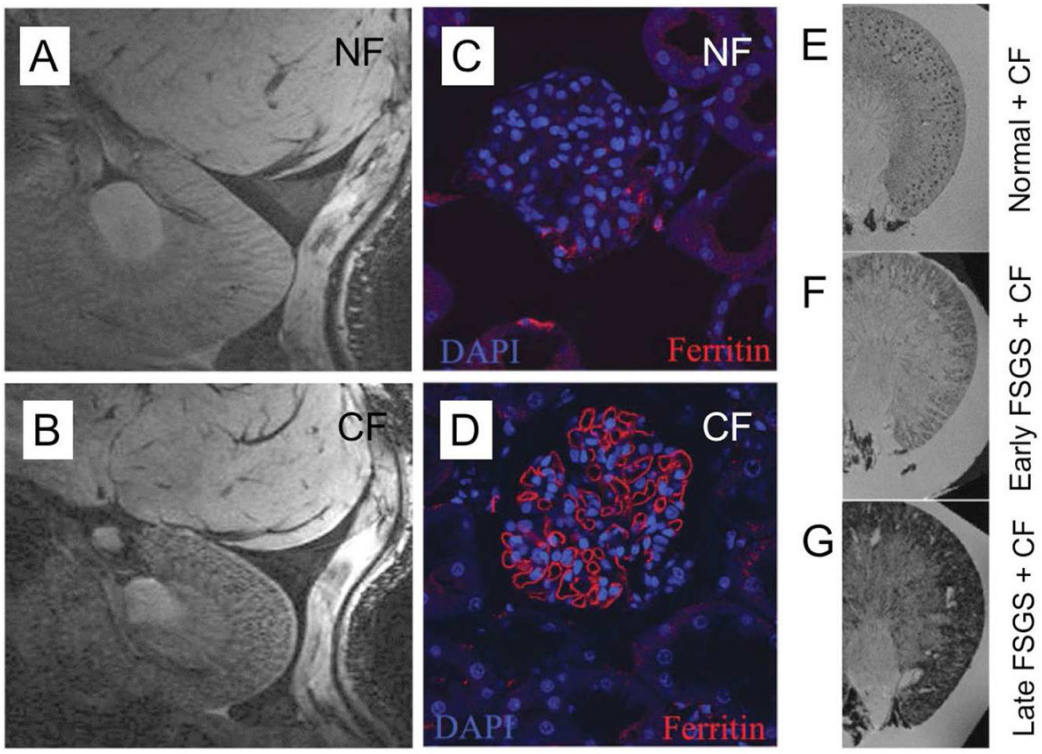


**Figure 6.**

Detecting the basement membrane in kidney glomeruli. MR images of the kidney of a rat acquired 1.5 hours after injection with A) NF and B) CF, with the speckled pattern of signal loss in B) indicating detection of glomeruli. Confocal microscopy images of sections of kidney of a rat injected with C) NF and D) CF, with the cell nuclei stained with DAPI (blue) and for ferritin (red). MR images of excised rat kidneys: E) normal injected with CF, F) early FSGS injected with CF and G) late FSGS injected with CF. Figure adapted with permission from reference [101].

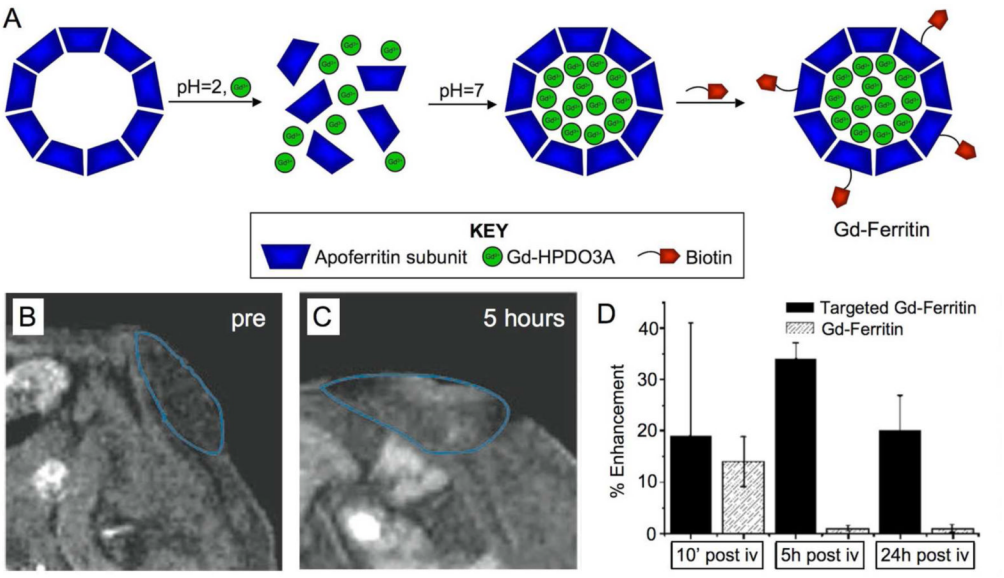


**Figure 7.**

A) Loading apoferritin with Gd-HPDO3A, a Gd3+-chelate, by reducing the pH to 2, to disassemble the apoferritin subunits, before raising the pH to 7 to trap Gd-HPDO3A in the apoferritin cavity. Biotin is subsequently attached to the nanoparticle surface to form Gd-ferritin. MR images of a tumor in a mouse pre (B) and 5 hours post (C) injection with targeted Gd-ferritin. D) Enhancement seen in tumors implanted in the flanks of mice injected with targeted or non-targeted Gd-ferritin. Figure adapted with permission from reference [107].